GEOPHYSICS, VOL. 79, NO. 6 (NOVEMBER-DECEMBER 2014); P. R233–R246, 15 FIGS., 1 TABLE.
10.1190/GEO2013-0456.1

Downloaded 10/21/14 to 146.23.3.251. Redistribution subject to SEG license or copyright; see Terms of Use at http://library.seg.org/

Stochastic inversion of seismic PP and PS data for reservoir parameter estimation

Jinsong Chen[1] and Michael E. Glinsky[2]

ABSTRACT

We have investigated the value of isotropic seismic converted-wave (i.e., PS) data for reservoir parameter estimation using stochastic approaches based on a floating-grain rock-physics model. We first performed statistical analysis on a simple two-layer model built on actual borehole logs and compared the relative value of PS data versus amplitude-variation-with-offset (AVO) gradient data for estimating the floating-grain fraction. We found that PS data were significantly more informative than AVO gradient data in terms of likelihood functions, and the combination of PS and AVO gradient data together with PP data provided the maximal value for the reservoir parameter estimation. To evaluate the value of PS data under complex situations, we developed a hierarchical Bayesian model to combine seismic PP and PS data and their associated time registration. We extended a model-based Bayesian method developed previously for inverting seismic PP data only, by including PS responses and time registration as additional data and PS traveltime and reflectivity as additional variables. We applied the method to a synthetic six-layer model that closely mimics real field scenarios. We found that PS data provided more information than AVO gradient data for estimating the floating-grain fraction, porosity, net-to-gross, and layer thicknesses when their corresponding priors were weak.

INTRODUCTION

Multicomponent seismic surveying has been used for hydrocarbon exploration for decades because it can capture the seismic wavefield more completely than conventional single-element techniques (Stewart et al., 2002). Although several types of energy conversion may occur when seismic waves pass through the underlying earth, transmitted or multiple conversions generally have much lower amplitudes than P-down and S-up reflections (Rodriguez-Saurez, 2000). Consequently, among many applications of multicomponent seismic data, the use of converted-wave or PS images receives much more attention (Stewart et al., 2002; Mahmoudian and Margrave, 2004; Veire and Landrø, 2006). However, the high acquisition cost of collecting multicomponent seismic data compared with conventional seismic surveys and the challenge in processing multicomponent data make the use of converted-wave data as a routine practice difficult.

The interest in using multicomponent seismic data again for hydrocarbon applications is inspired by recent advances in seismic data acquisition technologies, such as ocean-bottom seismometer techniques (e.g., ocean-based cables and ocean-based nodes) (Hardage et al., 2011; Pacal, 2012). With the use of new techniques, multicomponent seismic data can be collected more reliably compared with conventional seismic survey techniques. Another major reason for using multicomponent seismic data is the need to estimate spatially distributed ductile fraction (Glinsky et al., 2013) and to characterize fractures for unconventional resources because S-wave splitting provides an effective approach to image fracture orientation and density (Bale et al., 2013). There are many other successful applications of converted-wave data, such as time-lapse monitoring of geomechanical changes (Davis et al., 2013) and reservoir characterization (Brettwood et al., 2013).

In this study, we use stochastic approaches to investigate the value of converted-wave data for reservoir parameter estimation based on a floating-grain rock-physics model developed by DeMartini and Glinsky (2006). The model is well documented in Gunning and Glinsky (2007) and appropriate for porous sedimentary rocks in which some solid materials are "floating" or not involved in loading support because it can explain the observed variation in P-wave velocity versus density trends and the lack of variation in the P-wave velocity versus S-wave velocity trends. The rock-physics relationship can be modified and applied to unconventional shale

Manuscript received by the Editor 8 December 2013; revised manuscript received 8 June 2014; published online 17 October 2014.
[1]Lawrence Berkeley National Laboratory, Earth Sciences Division, Berkeley, California, USA. E-mail: jchen@lbl.gov.
[2]ION Geophysical, Houston, Texas, USA. E-mail: michael.glinsky@iongeo.com.
© 2014 Society of Exploration Geophysicists. All rights reserved.

Downloaded 10/21/14 to 146.23.3.251. Redistribution subject to SEG license or copyright; see Terms of Use at http://library.seg.org/

resource exploration as done by Glinsky et al. (2013), in which the media are considered as binary mixing of brittle and ductile materials and the ductile fraction plays the same role as the floating-grain fraction in this model.

We use stochastic methods in the study because they have many advantages over traditional deterministic approaches in reservoir parameter estimation using multiple geophysical data sets, especially when we deal with complex issues involving uncertainty (Chen et al., 2008). We start by analyzing a simple two-layer model by comparing the relative value of PS versus amplitude-variation-with-offset (AVO) gradient data for estimating a floating-grain fraction according to their likelihoods when rock-physics models and seismic data are subject to uncertainty. We then focus on more complicated cases involving multiple layers and develop a hierarchical Bayesian model to combine seismic PP and PS data and their associated time registration.

We extend the model-based Bayesian method developed by Gunning and Glinsky (2004) for inverting seismic PP data to allow isotropic converted-wave responses and PS event time registration as additional data. We use the same rock-physics models and Markov chain Monte Carlo (MCMC) sampling strategies as Gunning and Glinsky (2004). Because this study is built on the previous work, the subsequent descriptions will be focused on the new development and applications; the details of other parts can be found in Gunning and Glinsky (2004).

ROCK-PHYSICS MODEL AND ANALYSIS OF TWO-LAYER MODELS

Floating-grain rock-physics model

We use the floating-grain rock-physics model developed by DeMartini and Glinsky (2006) and Gunning and Glinsky (2007) to link reservoir parameters to seismic attributes. In the model, the subsurface is considered as a binary mixture of reservoir members (e.g., sand) and nonreservoir members (e.g., shale). For sand, we assume that some solid materials are floating in pore space and the seismic properties (i.e., seismic P- and S-wave velocity and density) can be characterized by two fundamental parameters: the loading depth z, which is a measure of effective pressure, and the floating-grain fraction x. The general model is given below as

$$V_P = a_{vp} + b_{vp}z + c_{vp}x + \varepsilon_{vp}, \tag{1}$$

Table 1. Sand and shale rock-physics model coefficients from actual borehole logs.

	Regression equations	Standard errors	Units
Sand	$V_P = 645 + 0.508z + 5490x$	105	m/s
	$V_S = -1220 + 0.894V_P$	69	m/s
	$\rho = 1.70 + 1.65 \times 10^{-4}V_P + 1.56x$	0.0149	g/cc
Shale	$V_P = -1640 + 0.946z$	145	m/s
	$V_S = -1030 + 0.801\,V_P$	63	m/s
	$\rho = 0.651\,V_P^{0.166}$	0.030	g/cc

$$V_s = a_{vs} + b_{vs}V_p + \varepsilon_{vs}, \tag{2}$$

and

$$\rho = a_\rho + b_\rho V_P + c_\rho x + \varepsilon_\rho, \tag{3}$$

where V_P, V_S, and ρ are the seismic P- and S-wave velocity and density, respectively; a_{vp}, b_{vp}, c_{vp}, a_{vs}, b_{vs}, a_ρ, b_ρ, and c_ρ are the fitting coefficients. Symbols ε_{vp}, ε_{vs}, and ε_ρ represent uncertainty associated with the regression equations. We assume that ε_{vp}, ε_{vs}, and ε_ρ have Gaussian distributions with zero mean and variance of σ_{vp}^2, σ_{vs}^2, and σ_ρ^2, respectively.

We rewrite equations 2 and 3 in terms of the loading depth z and the floating-grain fraction x as follows:

$$V_S = (a_{vs} + a_{vp}b_{vs}) + b_{vs}b_{vp}z + b_{vs}c_{vp}x + (b_{vs}\varepsilon_{vp} + \varepsilon_{vs}) \tag{4}$$

and

$$\rho = (a_\rho + a_{vp}b_\rho) + b_\rho b_{vp}z + (b_\rho c_{vp} + c_\rho)x + (b_\rho\varepsilon_{vp} + \varepsilon_\rho). \tag{5}$$

We can see that in the rock-physics model, seismic properties linearly depend on the reservoir parameters with uncertainty.

We can use different relationships for shale because seismic properties in shale do not depend on the floating-grain fraction. As in Gunning and Glinsky (2007), we drop the floating-grain fraction from equations 1 and 4 and use the power-law form of the Gardner relationship (Gardner et al., 1974) for density, i.e., $\rho = av_p^b + \varepsilon_\rho$, where a and b are fitting coefficients. By fitting actual borehole logs from suitable field sites, we can obtain all the needed coefficients and their associated standard errors for sand and shale members. Table 1 is a summary of all those values.

Reflectivity coefficients

We use the linearized Zoeppritz approximations (Aki and Richards, 1980) for small contrasts to obtain PP and PS reflectivity coefficients at an interface, which are given below as

$$R_{pp} = \frac{1}{2}\left(\frac{\Delta V_P}{V_P} + \frac{\Delta\rho}{\rho}\right) + \frac{1}{2}\left[\frac{\Delta V_P}{V_P} - 4r_{sp}^2\left(\frac{\Delta\rho}{\rho} + 2\frac{\Delta V_S}{V_S}\right)\right]\sin^2\theta_p + \frac{1}{2}\frac{\Delta V_P}{V_P}\sin^2\theta_p\tan^2\theta_p \tag{6}$$

and

$$R_{ps} = -\frac{\sin\theta_p}{2\cos\theta_s}(1 - 2r_{sp}^2\sin^2\theta_p + 2r_{sp}\cos\theta_p\cos\theta_s)\frac{\Delta\rho}{\rho} + \frac{2\sin\theta_p}{\cos\theta_s}(r_{sp}^2\sin^2\theta_p - r_{sp}\cos\theta_p\cos\theta_s)\frac{\Delta V_S}{V_S}, \tag{7}$$

where $V_P = (V_{P1} + V_{P2})/2$, $V_S = (V_{S1} + V_{S2})/2$, $\rho = (\rho_1 + \rho_2)/2$, $r_{sp} = V_S/V_P$, $\Delta V_P = V_{P2} - V_{P1}$, $\Delta V_S = V_{S2} - V_{S1}$, and $\Delta\rho = \rho_2 - \rho_1$, where ($V_{P1}$, V_{S1}, and ρ_1) and (V_{P2}, V_{S2}, and ρ_2) are the P- and S-wave velocity and density in the layers above and below the

Downloaded 10/21/14 to 146.23.3.251. Redistribution subject to SEG license or copyright; see Terms of Use at http://library.seg.org/

interface. Symbols θ_p and θ_s are the P- and S-wave incident angles; they are connected through Snell's law as $\sin\theta_p/V_P = \sin\theta_s/V_S$.

Equation 6 is the same as the one used by Castagna et al. (1998), in which the first and second terms on the right of the equation are referred to as AVO intercept and gradient, respectively. The third term is high-order variations and dominated at far offsets near the critical angle. Equation 7 is the same as the one used by Veire and Landrø (2006). For ease of description, we let A_0 be the AVO intercept, A_1 be all the terms on the right side of equation 7, and A_2 be the AVO gradient with the high-order term. Let

$$\begin{cases} g_1 = -\frac{\sin\theta_p}{2\cos\theta_s}(1 - 2r_{sp}^2\sin^2\theta_p + 2r_{sp}\cos\theta_p\cos\theta_s), & \text{and} \\ g_2 = \frac{2\sin\theta_p}{\cos\theta_s}(r_{sp}^2\sin^2\theta_p - r_{sp}\cos\theta_p\cos\theta_s). \end{cases} \tag{8}$$

We have the following relationship:

$$\begin{pmatrix} A_0 \\ A_1 \\ A_2 \end{pmatrix} = \begin{pmatrix} 1/2 & 1/2 & 0 \\ g_1 & 0 & g_2 \\ -2r_{sp}^2\sin^2\theta_p & \sin^2\theta_p(1+\tan^2\theta_p)/2 & -4r_{sp}^2\sin^2\theta_p \end{pmatrix} \times \begin{pmatrix} \Delta\rho/\rho \\ \Delta V_P/V_P \\ \Delta V_S/V_S \end{pmatrix}. \tag{9}$$

We use the letter $\mathbf{A}$ to represent the vector on the left side of equation 9 and use $\mathbf{M}_a$ and $\Delta\mathbf{C}$ to represent the matrix and the vector on the right side of the equation. Thus, equation 9 becomes $\mathbf{A} = \mathbf{M}_a\Delta\mathbf{C}$. These notations will be used in the subsequent text.

Synthetic two-layer model

To demonstrate the value of PS data, we start from a simple two-layer model based on actual borehole logs from Gunning and Glinsky (2007), with the first layer being shale and the second layer being sand whose rock-physics models are given in Table 1. Because we focus on estimation of the floating-grain fraction in the sand layer, we fix the loading depth as $z_1 = 5200$ m and $z_2 = 5321$ m for the first and second layers. By using the shale regression equations with coefficients given in Table 1, we have $V_{P1} = 3279$ m/s, $V_{S1} = 1596$ m/s, and $\rho_1 = 2.50$ g/cm^3. By using equations 1, 4, and 5, we get

$$\Delta\rho = (a_\rho + a_{vp}b_\rho + b_{vp}b_\rho z_2 - \rho_1) + (b_\rho c_{vp} + c_\rho)x + (\varepsilon_\rho + b_\rho\varepsilon_{vp}), \tag{10}$$

$$\Delta V_P = (a_{vp} + b_{vp}z_2 - V_{P1}) + c_{vp}x + \varepsilon_{vp}, \tag{11}$$

and

$$\Delta V_S = (a_{vs} + a_{vp}b_{vs} + b_{vp}b_{vs}z_2 - V_{S1}) + b_{vs}c_{vp}x + (\varepsilon_{vs} + b_{vs}\varepsilon_{vp}). \tag{12}$$

Let

$$\begin{cases} w_\rho = a_\rho + a_{vp}b_\rho + b_{vp}b_\rho z_2 - \rho_1, \\ w_{vp} = a_{vp} + b_{vp}z_2 - V_{P1}, \\ w_{vs} = a_{vs} + a_{vp}b_{vs} + b_{vp}b_{vs}z_2 - V_{S1}. \end{cases} \tag{13}$$

We have

$$\begin{pmatrix} \Delta\rho/\rho \\ \Delta V_P/V_P \\ \Delta V_S/V_S \end{pmatrix} = \begin{pmatrix} w_\rho/\rho \\ w_{vp}/V_P \\ w_{vs}/V_S \end{pmatrix} + \begin{pmatrix} (c_\rho + b_\rho c_{vp})/\rho \\ c_{vp}/V_P \\ b_{vs}c_{vp}/V_S \end{pmatrix} x + \begin{pmatrix} (\varepsilon_\rho + b_\rho\varepsilon_{vp})/\rho \\ \varepsilon_{vp}/V_P \\ (\varepsilon_{vs} + b_{vs}\varepsilon_{vp})/V_S \end{pmatrix}. \tag{14}$$

Let $\mathbf{W}_0$, $\mathbf{W}_1$, and $\boldsymbol{\varepsilon}_w$ represent the first, second, and third vectors on the right side of equation 14; thus, we have $\Delta\mathbf{C} = \mathbf{W}_0 + \mathbf{W}_1 x + \boldsymbol{\varepsilon}_w$. By assuming that the errors in equations 1–3 are independent, we can obtain the following covariance matrix $\boldsymbol{\Sigma}_w$:

$$\boldsymbol{\Sigma}_w = \begin{pmatrix} (\sigma_\rho^2 + b_\rho^2\sigma_{vp}^2)/\rho^2 & b_\rho\sigma_{vp}^2/(\rho V_P) & b_\rho b_{vs}\sigma_{vp}^2/(\rho V_S) \\ b_\rho\sigma_{vp}^2/(\rho V_P) & \sigma_{vp}^2/V_P^2 & b_{vs}\sigma_{vp}^2/(V_P V_S) \\ b_\rho b_{vs}\sigma_{vp}^2/(\rho V_S) & b_{vs}\sigma_{vp}^2/(V_P V_S) & (\sigma_{vs}^2 + b_{vs}^2\sigma_{vp}^2)/V_s^2 \end{pmatrix}. \tag{15}$$

Synthetic seismic data and likelihood function

For the purpose of this analysis, we consider PP and PS reflectivities at the interface as data even if they often are unknown and estimated from full-waveform seismic responses in practice. Specifically, we use a PP trace with a zero incident angle (i.e., A_0), a PS trace with the P-wave incident angle of 45° (i.e., A_1), and an AVO gradient trace (including the high-order term) with the P-wave incident angle of 45° (i.e., A_2). Let vector $\mathbf{R}_m$ be the data with additive Gaussian random noise $\boldsymbol{\varepsilon}_m$; we thus have

$$\begin{aligned} \mathbf{R}_m &= \mathbf{M}_d\mathbf{A} + \boldsymbol{\varepsilon}_m = \mathbf{M}_d\mathbf{M}_a\Delta\mathbf{C} + \boldsymbol{\varepsilon}_m \\ &= \mathbf{M}_d\mathbf{M}_a(\mathbf{W}_0 + \mathbf{W}_1 x) + (\boldsymbol{\varepsilon}_m + \mathbf{M}_d\mathbf{M}_a\boldsymbol{\varepsilon}_w), \end{aligned} \tag{16}$$

where $\mathbf{M}_d$ is referred to as a data matrix that determines which types of data are used for analysis (see Appendix A).

The second term on the right side of equation 16 is residuals; they include measurement errors in seismic data and uncertainty caused by rock-physics models. Because both the measurement errors and uncertainty in rock-physics models are assumed to have multivariate Gaussian distributions, their summation also has a multivariate Gaussian distribution (Stone, 1995). Let $\boldsymbol{\Sigma}_m$ be the covariance matrix of the measurement errors and $\boldsymbol{\Sigma}_w$ be the covariance matrix of the uncertainty in rock-physics models. The combined covariance thus is given by $\boldsymbol{\Sigma}_c = \boldsymbol{\Sigma}_m + (\mathbf{M}_d\mathbf{M}_a)\boldsymbol{\Sigma}_w(\mathbf{M}_d\mathbf{M}_a)^T$, where $\boldsymbol{\Sigma}_w$ is given by equation 15. Consequently, the likelihood function of x given data $\mathbf{R}_m$ is a multivariate Gaussian distribution as follows:

Downloaded 10/21/14 to 146.23.3.251. Redistribution subject to SEG license or copyright; see Terms of Use at http://library.seg.org/

$$f(\mathbf{R}_m|x) \propto \left|\boldsymbol{\Sigma}_c\right|^{-1/2} \times \exp\left\{-(\mathbf{R}_m - \mathbf{M}_d\mathbf{M}_a\mathbf{W}_0 - \mathbf{M}_d\mathbf{M}_a\mathbf{W}_1 x)^T\boldsymbol{\Sigma}_c^{-1} \times (\mathbf{R}_m - \mathbf{M}_d\mathbf{M}_a\mathbf{W}_0 - \mathbf{M}_d\mathbf{M}_a\mathbf{W}_1 x)\right\}. \quad (17)$$

Model comparison

We compare the estimation results obtained by using four combinations of seismic data by specifying the data matrices: (1) using the PP data only, (2) using the PP and PS data, (3) using the PP and AVO gradient data, and (4) using all the seismic data (see Appendix A). Their corresponding data are represented by $\mathbf{R}_m^{(1)}$, $\mathbf{R}_m^{(2)}$, $\mathbf{R}_m^{(3)}$, and $\mathbf{R}_m^{(4)}$. To avoid the effects of prior distribution on the floating-grain fraction, we focus on the likelihood functions $f(\mathbf{R}_m^{(k)}|x)$ ($k = 1, 2, 3,$ and 4) for those models.

Figure 1 compares the likelihood functions for the true floating-grain fraction being 0.0 (Figure 1a) and 0.035 (Figure 1b). The noise levels for all the data are equal to 0.01 in the unit of reflection coefficients (RFCs). As we expect, the true values have the maximum likelihood in both the cases. It is clear that the likelihoods of using the PP and AVO gradient data are considerably larger than those of using the PP data only. The likelihoods of using the PP and PS data are significantly larger than those of using the PP and AVO gradient data. This suggests that the combination of the PP and PS data is more informative for estimating the floating-grain fraction than the combination of the PP and AVO gradient data. When we use all the data, we get the largest likelihoods. This implies that the PS and AVO gradient data might complement each other to some degree. In addition, we can see that the clean sand (i.e., $x = 0$; see Figure 1a) overall has larger likelihoods than the sand with floating grain (i.e., $x = 0.035$; see Figure 1b).

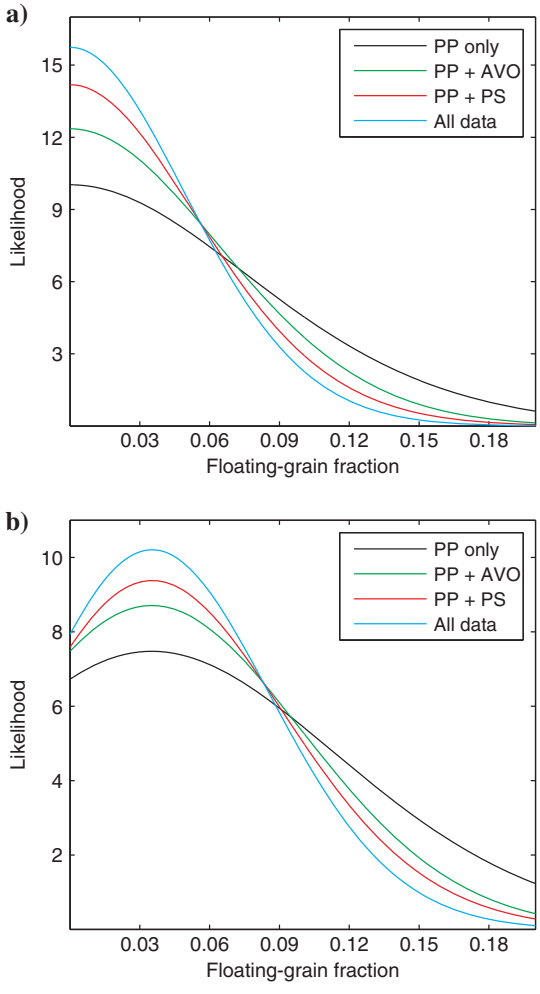

Figure 1. Likelihoods of the floating-grain fraction given various data combinations for the true value of (a) 0.0% and (b) 3.5%.

The above comparison may depend on noise levels in the seismic data. In practice, PS and AVO gradient data typically have larger errors than PP data. To investigate the effects of noise on the likelihood analysis, we vary noise levels in PS and AVO gradient data from 0.01 RFC to 0.1 RFC while still fixing the noise level of the PP data as 0.01 RFC. We first calculate the maximum likelihoods for each combination of seismic data and then normalize the results by the values of using the PP data only to get the following likelihood ratios as

$$r_k = \frac{\max\{f(\mathbf{R}_m^{(k)}|x)\}}{\max\{f(\mathbf{R}_m^{(1)}|x)\}}. \quad (18)$$

Figure 2 shows the likelihood ratios for the true floating-grain fraction of 0.0 and 0.035. Generally, as the noise levels in the PS and AVO gradient data increase, the likelihood ratios decrease and approach 1, the result of using the PP data only. Additionally, the likelihood ratios of using the PP and PS data always are larger than those of using the PP and AVO gradient data; the likelihood ratios of using all the data always have the largest values. This suggests that the combination of PP and PS data is more informative than that of PP and AVO gradient data even under large noise levels.

BAYESIAN MODEL FOR MULTIPLE LAYERS

Hierarchical Bayesian models

Although analysis of two-layer models allows us to understand the value of PS data for floating-grain fraction estimation, it is marginal analysis of relative changes of compaction and floating-grain fraction across an interface under simple conditions. In the case of multiple layers, we need to develop a hierarchical Bayesian model to combine seismic PP and PS data and their time registration. This model is an extension of the model-based Bayesian method by Gunning and Glinsky (2004) with converted-wave responses and PS time registration as additional data and PS traveltime and reflectivity as additional unknowns.

We consider effective seismic P- and S-wave velocities, V_P and V_S, density $\boldsymbol{\rho}$, and seismic PP and PS reflectivities, $\mathbf{R}_{pp}$ and $\mathbf{R}_{ps}$ as unknowns. They are functions of rock-physics parameters through suitable rock-physics models. We consider PP traveltime $\mathbf{t}_{pp}$ as a primary unknown; the layer thickness $\mathbf{d}$ and PS traveltime $\mathbf{t}_{ps}$ can be derived from the PP traveltime and associated effective seismic attributes. The data used for inversion include seismic PP and PS full-waveforms $\mathbf{S}_{pp}$ and $\mathbf{S}_{ps}$ and PP and PS event registration time ($\mathbf{T}_{pp}$ and $\mathbf{T}_{ps}$). If available, we can also include other types of information from nearby boreholes, such as depth constraints $\mathbf{D}_b$.

Downloaded 10/21/14 to 146.23.3.251. Redistribution subject to SEG license or copyright; see Terms of Use at http://library.seg.org/

Figure 3 shows all the unknowns, available data, and their relationships; the dashed rectangle highlights our extension to the method by Gunning and Glinsky (2004). Specifically, we add two unknowns related to the converted wave (i.e., $\mathbf{t}_{ps}$ and $\mathbf{R}_{ps}$) and two types of new data sets (i.e., $\mathbf{T}_{ps}$ and $\mathbf{S}_{ps}$). Following the direct graphical model, we have the hierarchical Bayesian model:

$$\begin{aligned} f(\boldsymbol{\alpha}, \mathbf{t}_{pp}, \mathbf{t}_{ps}, \mathbf{d}, \mathbf{v}_p, \mathbf{v}_s, \boldsymbol{\rho}, \mathbf{R}_{pp}, \mathbf{R}_{ps} | \mathbf{S}_{pp}, \mathbf{S}_{ps}, \mathbf{T}_{pp}, \mathbf{T}_{ps}, \mathbf{D}_b) \\ \propto f(\mathbf{S}_{pp}|\mathbf{t}_{pp}, \mathbf{R}_{pp}) f(\mathbf{S}_{ps}|\mathbf{t}_{ps}, \mathbf{R}_{ps}) f(\mathbf{T}_{pp}|\mathbf{t}_{pp}) \\ \times f(\mathbf{T}_{ps}|\mathbf{t}_{ps}) f(\mathbf{D}_b|\mathbf{d}) f(\mathbf{R}_{pp}|\mathbf{v}_p, \mathbf{v}_s, \boldsymbol{\rho}) \\ \times f(\mathbf{R}_{ps}|\mathbf{v}_p, \mathbf{v}_s, \boldsymbol{\rho}) f(\mathbf{d}|\mathbf{t}_{pp}, \mathbf{v}_p) f(\mathbf{t}_{ps}|\mathbf{t}_{pp}, \mathbf{v}_p, \mathbf{v}_s) \\ \times f(\mathbf{v}_p, \mathbf{v}_s, \boldsymbol{\rho}|\boldsymbol{\alpha}) f(\boldsymbol{\alpha}) f(\mathbf{t}_{pp}). \end{aligned} \tag{19}$$

Equation 19 defines a joint posterior probability distribution function of all unknown parameters up to a normalizing constant. The first five terms on the right side of the equation are the likelihood functions of available data, which link data to the associated unknowns; the other terms on the right side are the prior probability distributions, which are derived from other sources of information, such as rock-physics models. We define all the likelihood functions and prior distributions in a similar way to the method of Gunning and Glinsky (2004). In the following, we only describe the new development.

Equation 19 is a general Bayesian model for combining seismic PP and converted-wave data; we can simplify or vary the equation in different ways depending on specific applications. For example, we can consider PP and PS reflectivities as functions of $\mathbf{v}_p$, $\mathbf{v}_s$, and $\boldsymbol{\rho}$, but ignore their associated uncertainties. We can also consider depth $\mathbf{d}$ as a function of P-wave velocity and PP traveltime. Because in Bayesian statistics (Bernardo and Smith, 2000) data affect unknowns only through likelihood functions, we can use some statistics $\mathbf{Q}(\mathbf{S}_{pp}, \mathbf{S}_{ps})$ of seismic data $\mathbf{S}_{pp}$ and $\mathbf{S}_{ps}$ in the Bayesian model, e.g., the rotation and truncation of original seismic data through principal component analysis (Venables and Ripley, 1999) or other methods. Consequently, we can have the following Bayesian model:

$$\begin{aligned} f(\boldsymbol{\alpha}, \mathbf{t}_{pp}, \mathbf{t}_{ps}, \mathbf{v}_p, \mathbf{v}_s, \boldsymbol{\rho}|\mathbf{S}_{pp}, \mathbf{S}_{ps}, \mathbf{T}_{pp}, \mathbf{T}_{ps}) \\ \propto f(\mathbf{Q}|\mathbf{t}_{pp}, \mathbf{t}_{ps}, \mathbf{v}_p, \mathbf{v}_s, \boldsymbol{\rho}) f(\mathbf{T}_{pp}|\mathbf{t}_{pp}) f(\mathbf{T}_{ps}|\mathbf{t}_{ps}) \\ \times f(\mathbf{t}_{ps}|\mathbf{t}_{pp}, \mathbf{v}_p, \mathbf{v}_s) f(\mathbf{v}_p, \mathbf{v}_s, \boldsymbol{\rho}|\boldsymbol{\alpha}) f(\boldsymbol{\alpha}) f(\mathbf{t}_{pp}). \end{aligned} \tag{20}$$

Likelihood function of seismic data

We describe a general form of the likelihood function in terms of statistics of seismic data, with the likelihood function of original seismic data as a special case of the form. Let $\mathbf{G}(\mathbf{t}_{pp}, \mathbf{t}_{ps}, \mathbf{v}_p, \mathbf{v}_s, \boldsymbol{\rho})$ be the response vector of a suitable forward model that links seismic statistics $\mathbf{Q}$ to unknowns. Let vector $\boldsymbol{\varepsilon}_m$ represent the residuals. We assume that the residuals have the multivariate Gaussian distribution with zero mean and the covariance matrix of $\boldsymbol{\Sigma}_m$; thus, we have

$$\begin{aligned} f(\mathbf{Q}|\mathbf{t}_{pp}, \mathbf{t}_{ps}, \mathbf{v}_p, \mathbf{v}_s, \boldsymbol{\rho}) = (2\pi)^{-k/2} \left|\boldsymbol{\Sigma}_m\right|^{-1/2} \\ \times \exp\left(-\frac{1}{2}(\mathbf{Q} - \mathbf{G}(\mathbf{t}_{pp}, \mathbf{t}_{ps}, \mathbf{v}_p, \mathbf{v}_s, \boldsymbol{\rho}))^T \boldsymbol{\Sigma}_m^{-1} \right. \\ \left. \times (\mathbf{Q} - \mathbf{G}(\mathbf{t}_{pp}, \mathbf{t}_{ps}, \mathbf{v}_p, \mathbf{v}_s, \boldsymbol{\rho}))\right), \end{aligned} \tag{21}$$

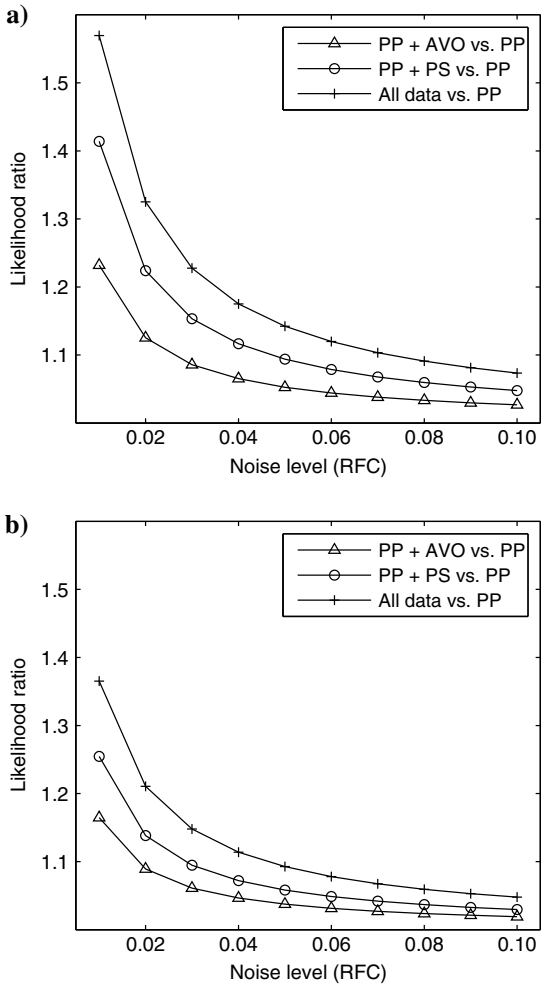

Figure 2. Likelihood ratios of using various combinations of seismic data compared with that of using PP data only as a function of measurement errors in PS and AVO gradient data for the true value of (a) 0.0% and (b) 3.5%.

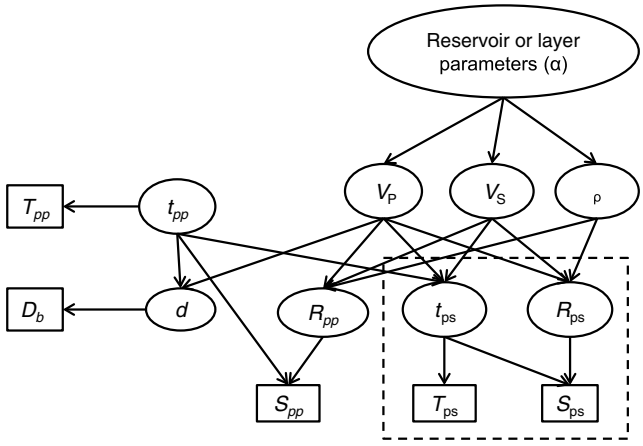

Figure 3. Dependent relationships among unknown parameters and data.

Downloaded 10/21/14 to 146.23.3.251. Redistribution subject to SEG license or copyright; see Terms of Use at http://library.seg.org/

where k is the dimension of the multivariate Gaussian distribution and $|\mathbf{\Sigma}_m|$ is the determinant of the covariance matrix $\mathbf{\Sigma}_m$. One of the main advantages of using statistics in equation 21 is that we can have more options in defining likelihood functions so that we can make their residuals uncorrelated.

Likelihood functions of PP and PS event time registration

The use of event time registration as data is one of the main advantages of the method by Gunning and Glinsky (2004), as well as the current extension, because the PP event time is directly related to the P-wave velocity and the PS event time is directly related to P- and S-wave velocities. They provide additional information to constrain the estimates of P- and S-wave velocities beyond the reflectivity-based PP and PS full waveforms.

Traditional methods for joint inversion of PP and PS data are primarily based on the mapping of PS data to PP time (or domain conversion), in which PS data are considered as additional seismic stacks. Although this approach is simple to implement, it suffers from difficulties such as wavelet distortion (Bansal and Matheney, 2010) because the conversion of PS time to PP time needs interval seismic P-to-S velocity ratios, which are not known a priori.

In this study, we avoid the PP-to-PS domain conversion and use PS data directly in the PS time domain. We pick a PS event from PS seismograms that has a good correspondence with a PP event in the PP seismograms along the same profile; we refer to it as the master PS horizon. In the PS forward simulation, we calculate all the PS times relative to the master horizon. The relative PP and PS time for a given layer is calculated by

$$\Delta t_{\mathrm{ps}} = \frac{1}{2}\left(1+\frac{V_{\mathrm{P}}}{V_{\mathrm{S}}}\right)\Delta t_{\mathrm{pp}}, \tag{22}$$

where V_{P} and V_{S} are interval velocities and are unknown; they will be estimated in inversion procedures.

The likelihood functions of PP and PS event registration time are determined by assuming that the errors have multivariate Gaussian distributions. Let $\mathbf{\Sigma}_{\mathrm{pp}}$ and $\mathbf{\Sigma}_{\mathrm{ps}}$ be the covariance matrices of PP and PS event time, respectively. We have the following likelihood functions:

$$f(\mathbf{T}_{\mathrm{pp}}|\mathbf{t}_{\mathrm{pp}}) = (2\pi)^{-k_1/2}\left|\mathbf{\Sigma}_{\mathrm{pp}}\right|^{-1/2}\exp\left(-\frac{1}{2}(\mathbf{T}_{\mathrm{pp}}-\mathbf{t}_{\mathrm{pp}})^T\mathbf{\Sigma}_{\mathrm{pp}}^{-1}(\mathbf{T}_{\mathrm{pp}}-\mathbf{t}_{\mathrm{pp}})\right)$$

and

$$f(\mathbf{T}_{\mathrm{ps}}|\mathbf{t}_{\mathrm{ps}}) = (2\pi)^{-k_2/2}\left|\mathbf{\Sigma}_{\mathrm{ps}}\right|^{-1/2}\exp\left(-\frac{1}{2}(\mathbf{T}_{\mathrm{ps}}-\mathbf{t}_{\mathrm{ps}})^T\mathbf{\Sigma}_{\mathrm{ps}}^{-1}(\mathbf{T}_{\mathrm{ps}}-\mathbf{t}_{\mathrm{ps}})\right), \tag{23}$$

where k_1 and k_2 are the dimensions of $\mathbf{T}_{\mathrm{pp}}$ and $\mathbf{T}_{\mathrm{ps}}$; $|\mathbf{\Sigma}_{\mathrm{pp}}|$ and $|\mathbf{\Sigma}_{\mathrm{ps}}|$ are the determinants of the covariance matrix $\mathbf{\Sigma}_{\mathrm{pp}}$ and $\mathbf{\Sigma}_{\mathrm{ps}}$.

Conditionals of unknowns and Markov chain Monte Carlo sampling methods

We use MCMC methods to draw many samples from the joint distribution given in equation 20. To do this, we first need to derive conditional distributions of each type of unknowns given all other variables and data. The normalizing constants of each conditional are irrelevant when we use MCMC methods to draw samples. Therefore, we only need to keep the term on the right side of equation 20 to get its conditional, which is given below:

$$f(\mathbf{t}_{\mathrm{pp}}|\cdot) \propto f(\mathbf{Q}|\mathbf{t}_{\mathrm{pp}},\mathbf{t}_{\mathrm{ps}},\mathbf{v}_{\mathrm{p}},\mathbf{v}_{\mathrm{s}},\boldsymbol{\rho})f(\mathbf{T}_{\mathrm{pp}}|\mathbf{t}_{\mathrm{pp}})f(\mathbf{t}_{\mathrm{ps}}|\mathbf{t}_{\mathrm{pp}},\mathbf{v}_{\mathrm{p}},\mathbf{v}_{\mathrm{s}})f(\mathbf{t}_{\mathrm{pp}}), \tag{24}$$

$$f(\mathbf{t}_{\mathrm{ps}}|\cdot) \propto f(\mathbf{Q}|\mathbf{t}_{\mathrm{pp}},\mathbf{t}_{\mathrm{ps}},\mathbf{v}_{\mathrm{p}},\mathbf{v}_{\mathrm{s}},\boldsymbol{\rho})f(\mathbf{T}_{\mathrm{ps}}|\mathbf{t}_{\mathrm{ps}})f(\mathbf{t}_{\mathrm{ps}}|\mathbf{t}_{\mathrm{pp}},\mathbf{v}_{\mathrm{p}},\mathbf{v}_{\mathrm{s}}), \tag{25}$$

$$f(\mathbf{v}_{\mathrm{p}},\mathbf{v}_{\mathrm{s}},\boldsymbol{\rho}|\cdot) \propto f(\mathbf{Q}|\mathbf{t}_{\mathrm{pp}},\mathbf{t}_{\mathrm{ps}},\mathbf{v}_{\mathrm{p}},\mathbf{v}_{\mathrm{s}},\boldsymbol{\rho})f(\mathbf{t}_{\mathrm{ps}}|\mathbf{t}_{\mathrm{pp}},\mathbf{v}_{\mathrm{p}},\mathbf{v}_{\mathrm{s}})f(\mathbf{v}_{\mathrm{p}},\mathbf{v}_{\mathrm{s}},\boldsymbol{\rho}|\boldsymbol{\alpha}), \tag{26}$$

and

$$f(\boldsymbol{\alpha}|\cdot) \propto f(\mathbf{v}_{\mathrm{p}},\mathbf{v}_{\mathrm{s}},\boldsymbol{\rho}|\boldsymbol{\alpha})f(\boldsymbol{\alpha}). \tag{27}$$

For equations 24–26, we cannot obtain analytical forms of those conditionals because PP and PS registration time and seismic attributes $\mathbf{v}_{\mathrm{p}}$, $\mathbf{v}_{\mathrm{s}}$, and $\boldsymbol{\rho}$ are nonlinear functions of other variables. We have to use MCMC methods to draw many samples from the joint posterior distribution.

In equation 27, we use the floating-grain rock-physics model given in equations 1–3 to link layered seismic attributes to their corresponding reservoir parameters, which is a linear function in this case. Let vector $\mathbf{r}$ be the combined vector of $\mathbf{v}_{\mathrm{p}}$, $\mathbf{v}_s$, and $\boldsymbol{\rho}$ arranged by the layer indices and vector $\boldsymbol{\alpha}$ be the corresponding reservoir parameters. We thus have $\mathbf{r} = \boldsymbol{\mu}_r + \mathbf{H}\boldsymbol{\alpha} + \boldsymbol{\varepsilon}_r$, where vector $\boldsymbol{\varepsilon}_r$ represents the uncertainty associated with the linear relationship. We assume that it has a multivariate Gaussian distribution with zero mean and the covariance matrix of $\mathbf{\Sigma}_r$. The detailed derivation and specific forms are given in Appendix B.

If we use a multivariate Gaussian prior for $\boldsymbol{\alpha}$, i.e., $f(\boldsymbol{\alpha}) \sim N(\boldsymbol{\mu}_p, \mathbf{\Sigma}_p)$, we can obtain the analytical formula of posterior distribution, $f(\boldsymbol{\alpha}|\cdot) \sim N(\boldsymbol{\mu}_u, \mathbf{\Sigma}_u)$, which is given below as

$$\begin{cases} \mathbf{\Sigma}_u^{-1} = \mathbf{H}^T\mathbf{\Sigma}_r^{-1}\mathbf{H} + \mathbf{\Sigma}_p^{-1}, \\ \mathbf{\Sigma}_u^{-1}\boldsymbol{\mu}_u = \mathbf{H}^T\mathbf{\Sigma}_r^{-1}(\mathbf{r}-\boldsymbol{\mu}_r) + \mathbf{\Sigma}_p^{-1}\boldsymbol{\mu}_p. \end{cases} \tag{28}$$

We can obtain many samples of the joint posterior distribution given in equation 20 by using MCMC sampling methods.

CASE STUDY OF MULTIPLE LAYERS

We use the second example of Gunning and Glinsky (2007) to demonstrate the benefits of including converted-wave data into estimation of the floating-grain fraction. Figure 4 shows various logs from an actual borehole, including P- and S-wave velocities, densities, P- and S-wave velocity ratios, and P-wave impedance. According to the logs, we can build a synthetic model with six layers, which are (1) hard marl, (2) soft marl, (3) shale, (4) upper sand, (5) shale, and (6) lower sand, from shallow to deep (see Figure 4). Upper and lower sands are oil reservoirs with an oil saturation of 0.62, net-to-gross (NG) of 0.65, and thicknesses of 213 m (or 700 ft) and 110 m (or 360 ft), respectively. Figure 5 shows the blockwise

values of P- and S-wave velocities, densities, P- and S-wave velocity ratios, and P-wave impedance as a function of normalized depth. As shown in the figure, layers 4 and 6 have relatively low V_P/V_S ratios, both of which include the floating-grain fraction of 0.035.

PP and PS reflectivities and synthetic seismic data

We generate synthetic PP and PS data by first using equations 6 and 7 to calculate PP and PS reflectivities and then convolve the reflectivities with a 30-Hz Ricker wavelet. We consider P-wave incident angles of 0°, 9°, 18°, 27°, 36°, and 45°. Figure 6 shows the synthetic seismic data without noise added, in which PP data are in the PP time domain, but the PS data are in the PS time domain. For inversion, we consider the PP trace at the incident angle of zero as PP data and the PS traces at all the five incident angles as PS data. We extract AVO gradient traces by subtracting the zero incident angle PP trace from the PP traces with nonzero incident angles. We assume that all those data have uncorrelated Gaussian random noise with the standard deviation of 0.01 RFC or 0.02 RFC, depending on synthetic cases.

Priors for the inversion

Because our main focus is on the demonstration of the value of PS data for reservoir parameter estimation, we mainly focus on estimation of the floating-grain fraction and NG in the upper and

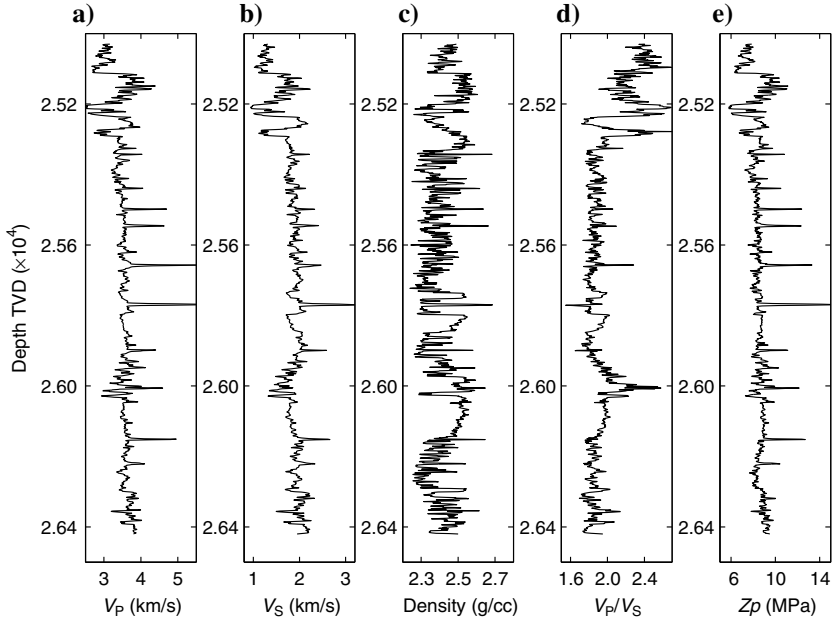

Figure 4. Various logs from an actual borehole as a function of depth: (a) P-wave velocity (km/s), (b) S-wave velocity (km/s), (c) density (g/cm^3), (d) V_P/V_S, and (e) P-impedance (MPa).

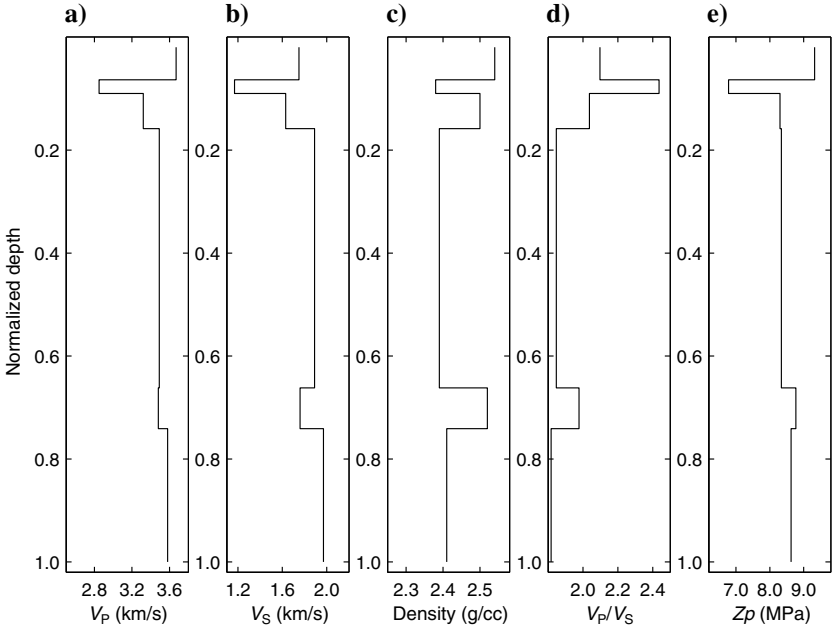

Figure 5. Blocked values obtained from the borehole logs using Backus average as a function of relative depth: (a) P-wave velocity (km/s), (b) S-wave velocity (km/s), (c) density (g/cm^3), (d) V_P/V_S, and (e) P-impedance (MPa).

Downloaded 10/21/14 to 146.23.3.251. Redistribution subject to SEG license or copyright; see Terms of Use at http://library.seg.org/

Downloaded 10/21/14 to 146.23.3.251. Redistribution subject to SEG license or copyright; see Terms of Use at http://library.seg.org/

lower pay layers. Similar to Gunning and Glinsky (2007), we first consider prior $X \sim N(0.02, 0.03^2)$; this is a strong prior for the true floating-grain fraction of 0.035. Second, we consider a weak prior $X \sim N(0.0, 0.05^2)$; this gives significant prior probability to the zero floating-grain fraction or clean sand. For the NG, we also consider two types of priors: (1) NG $\sim N(0.6, 0.1^2)$ and (2) NG$\sim N(0.5, 0.3^2)$.

Because we use model-based inversion methods, we can set a wide range of priors and consider many parameters as unknowns. For example, we assume that PP traveltime to each interface has the normal distribution with the true values as mean and 10 ms as the standard deviation. We assume that the uncertainty in the thickness of layer 4 is 21 m (or 70 ft) (i.e., 10% of the thickness) and 6 m (or 20 ft) for other layers.

Inversion cases

To test the usefulness of PS data for improving parameter estimation, we invert synthetic seismic data under the following four scenarios: (1) using only the PP data, (2) using PP and AVO gradient data, (3) using PP and PS data, and (4) using all the seismic data. We compare the posterior estimates of unknowns under each case with their corresponding prior distributions to evaluate the benefit of using PS data.

Because the above comparisons usually depend on an inversion situation, we consider the following three factors: (1) prior on the floating-grain fraction (i.e., $X \sim N(0.02, 0.03^2)$ or $X \sim N(0.0, 0.05^2)$), (2) prior on NG (i.e., NG $\sim N(0.6, 0.1^2)$ or NG $\sim N(0.5, 0.3^2)$), and (3) noise levels. We consider two sets of noise levels. The first one is that all seismic data have a noise level of 0.01 RFC, and the other is that the PP data has a noise level of 0.01 RFC, but other data have a noise level of 0.02 RFC.

By changing priors and noise levels, we obtain many sets of posterior distributions. We use MCMC methods to draw 20,000 samples and keep the later half for analysis (i.e., 10,000 samples). As an example, Figure 7 shows 200 realizations, selected from the 10,000 samples by keeping every 50th draw of the chain, for effective P- and S-wave velocity and density along the profile in the case using strong priors (i.e., $X \sim N(0.02, 0.03^2)$ and NG $\sim N(0.6, 0.1^2)$) and PP and PS data, in which the red line segments are their corresponding true values. Although those realizations are around the true values, considerable uncertainties exist. With the use of those samples, we can obtain wide ranges of statistics, such as means, medians, modes, density functions, and predictive intervals. In the following several subsections, we selectively report our inversion results.

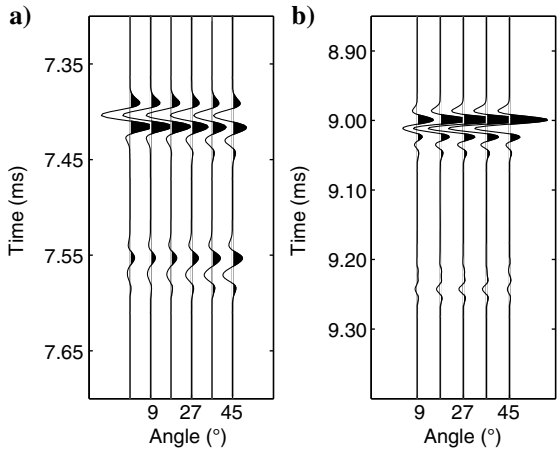

Figure 6. Synthetic seismic (a) PP and (b) PS data as a function of P-wave incident angles.

Estimation of floating-grain fraction, porosity, and net-to-gross

We compare the estimates of reservoir parameters (i.e., floating-grain fraction, NG, and porosity) under different prior distributions. To investigate the effects of priors about the floating-grain fraction, we use a strong prior about NG, i.e., NG $\sim N(0.6, 0.1^2)$, and noise levels for all the data types of 0.01 RFC. This implies the same quality for all the seismic data. We will explore the effects of noise levels later on.

Figure 8 compares the posterior probability densities (PDFs) of the floating-grain fraction, porosity, and NG with their corresponding prior PDFs for layer 4 (i.e., upper pay layer). For the floating-grain fraction, even under the good prior (i.e., $X \sim N(0.02, 0.03^2)$), the mode of the prior probability corresponds to the zero floating-grain fraction or clean sand. After conditioning to seismic data (i.e., PP data, PP plus AVO data, or PP plus PS data), the modes of the posterior PDFs correspond to the true values 0.035, with the results of using PP and PS data fitting better than the other two. As shown in Figure 9a, if we use a biased prior to clean sand, say $X \sim N(0.0, 0.05^2)$, the posterior estimates of the floating-grain fraction using PP data only and using PP and AVO gradient data provide biased results (i.e., clean sand). However, the combination of PP and PS data still provides correct estimates of the true value.

We can get similar results for comparison of porosity PDFs. Under the good prior of the floating-grain fraction, the modes of the posterior estimates for all the combinations of seismic data correspond to the true value well (see Figure 8b). But under the biased prior of the floating-grain fraction, only the posterior estimates

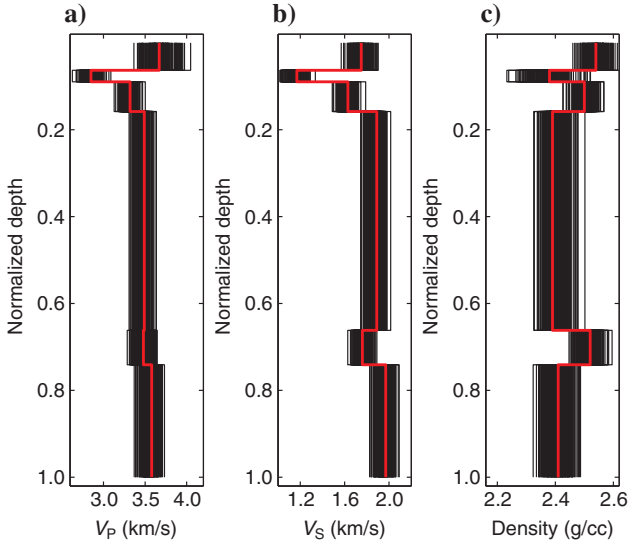

Figure 7. Selected realizations of effective (a) P-wave and (b) S-wave velocity and (c) density using a thinning of 50 from the 10,000 samples, in which the red line segments are the true values.

Downloaded 10/21/14 to 146.23.3.251. Redistribution subject to SEG license or copyright; see Terms of Use at http://library.seg.org/

obtained using PP and PS data provide good estimates of porosity (see Figure 9b). Because we use a very strong prior about the NG (i.e., NG $\sim N(0.6, 0.1^2)$) for the true value of 0.65, we expect the updating of the prior to be minimal for all the posterior estimates (Figure 9c).

We have similar comparisons of posterior PDFs for the lower pay layer (i.e., layer 6). As shown in Figure 10, although overall the posterior estimates of the floating-grain fraction and porosity are worse than those in the upper pay layer, the combination of PP and PS data provides more information than PP data only or the combination of PP and AVO gradient data for updating the priors of the floating-grain fraction and porosity.

Effects of the prior about net-to-gross and noise levels in seismic data

To explore the effects of the prior about NG, we use less informative prior (i.e., NG $\sim N(0.5, 0.3^2)$) for NG and good prior about the floating-grain fraction ($X \sim N(0.02, 0.03^2)$). Because the properties in the lower pay layer are much less sensitive to seismic data, we only do the comparison for the upper pay layer. Similar to what we found earlier, the combination of PP and PS data significantly improve the estimates of the floating-grain fraction and porosity. Unlike the previous comparison in Figures 8c and 9c, we found the combined use of PP and PS data in this case significantly improve the estimates of NG when it has significant uncertainty (see Figure 11c).

In reality, it is more difficult to collect and process PS and AVO gradient data compared with PP data. Therefore, they are likely subject to larger noise. To explore the effects of noise levels on reservoir parameter estimation, we let the prior of the floating-grain fraction be $X \sim N(0.02, 0.03^2)$ and let NG prior be NG$\sim N(0.6, 0.1^2)$. We set the noise level in the PP data still as 0.01 RFC but noise levels in the PS and AVO gradient data as 0.02 RFC. Figure 12 shows the posterior PDFs of the floating-grain frac-

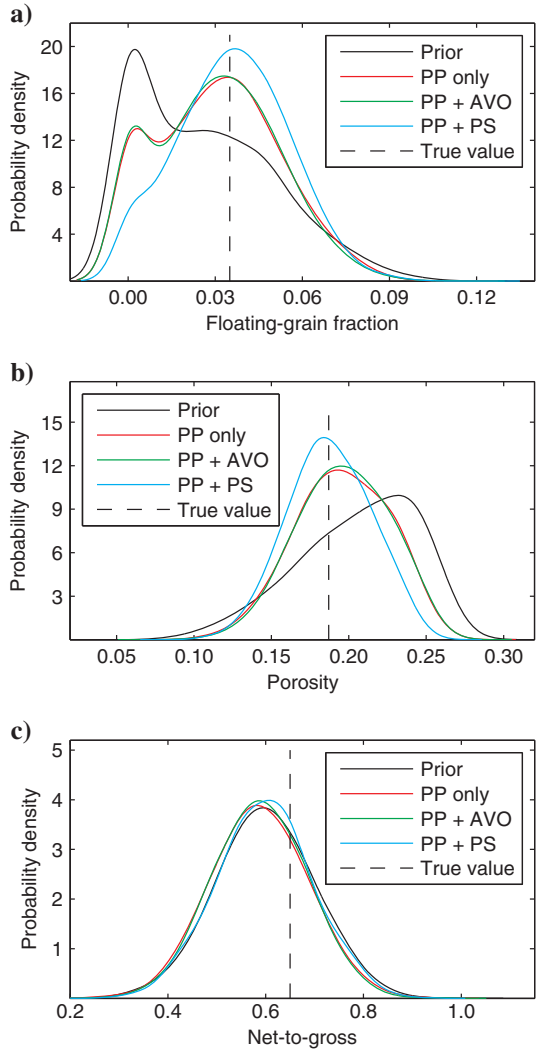

Figure 8. Posterior probability distributions of the (a) floating-grain fraction, (b) porosity, and (c) NG in the upper sand layer when priors about the floating-grain fraction and NG are strong (i.e., $X \sim N(0.02, 0.03^2)$ and NG $\sim N(0.6, 0.1^2)$, the reference case).

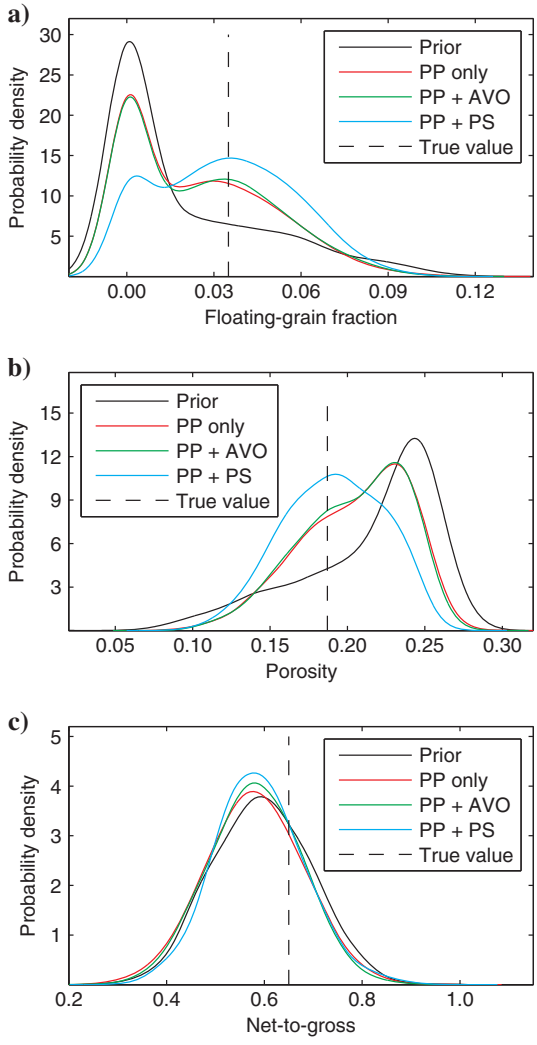

Figure 9. Posterior probability distributions of the (a) floating-grain fraction, (b) porosity, and (c) NG in the upper sand layer when the prior about the floating-grain fraction is weak (i.e., $X \sim N(0.0, 0.05^2)$).

Downloaded 10/21/14 to 146.23.3.251. Redistribution subject to SEG license or copyright; see Terms of Use at http://library.seg.org/

tion, porosity, and NG. Although the estimated results are slightly worse than those obtained using noise levels of 0.01 RFC for all the seismic data (see Figure 8), the conclusions remain the same.

Comparison of discrepancies between the estimated and the true values

Because we use sampling-based methods for inversion, we can obtain many samples of other variables as given in equation 20, such as effective P- and S-wave velocities, densities, layer-thickness, etc. With the use of those samples, we can not only visually compare prior and posterior PDFs but also calculate a wide range of statistics. In the previous comparisons, we qualitatively compare the posterior estimates with their corresponding priors. To demonstrate the value of PS data, in this subsection, we quantitatively compare the estimated results with their corresponding true values.

We first compare the difference between the estimated median and the true value, which measures how accurate a chosen point estimator (in this case, median) to the true value of a given parameter. Figure 13a compares the differences between the estimated floating-grain fraction, porosity, and NG values with their true values. The prior for the floating-grain fraction is $X \sim N(0.0, 0.05^2)$ and for NG is $\mathrm{NG} \sim N(0.6, 0.1^2)$, and the noise levels are 0.01 RFC for PP data and 0.02 for other data sets. We normalize the results by the difference obtained from prior distributions. For NG, as we demonstrated earlier, under the good prior, the estimated medians do not improve the prior medians. The value slightly more than 1.0 may reflect the effects of noise in seismic data or sampling variations during the inversion procedure. For the floating-grain fraction and porosity, when conditioning to PP data, the differences are significantly reduced. When adding AVO gradient data, the improvement is minimal, but adding PS data leads to further reduction.

Figure 13b compares the differences for effective P- and S-wave velocities, effective density, and layer thickness. For effective P-wave velocity and density, conditioning to PP data significantly improves the accuracy, and further adding AVO gradients or PS data does not lead to a significant reduction. However, for estimation of effective S-wave velocity and layer thickness, either adding AVO

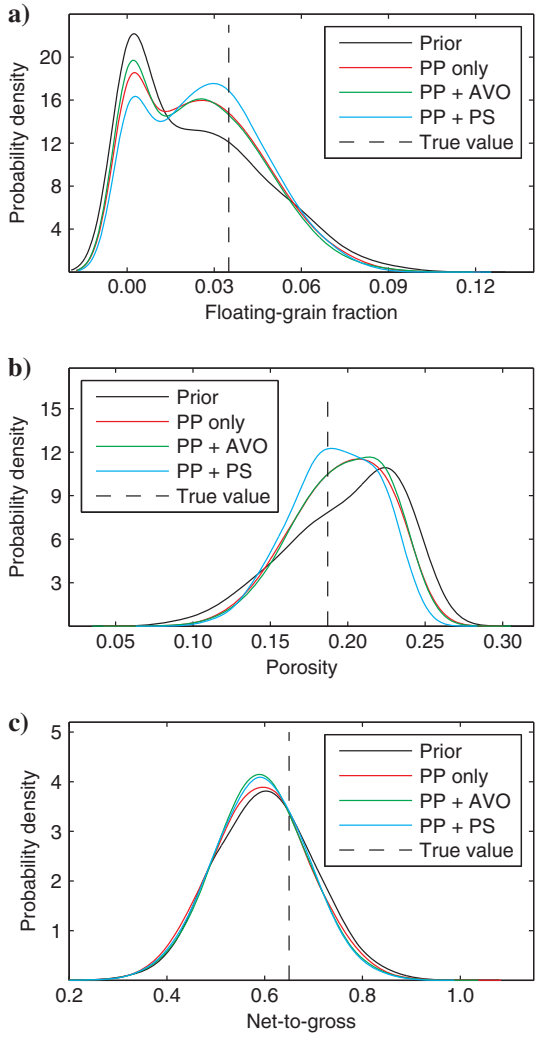

Figure 10. Posterior probability distributions of the (a) floating-grain fraction, (b) porosity, and (c) NG in the lower sand layer when priors about the floating-grain fraction and NG are strong (i.e., $X \sim N(0.02, 0.03^2)$ and $\mathrm{NG} \sim N(0.6, 0.1^2)$).

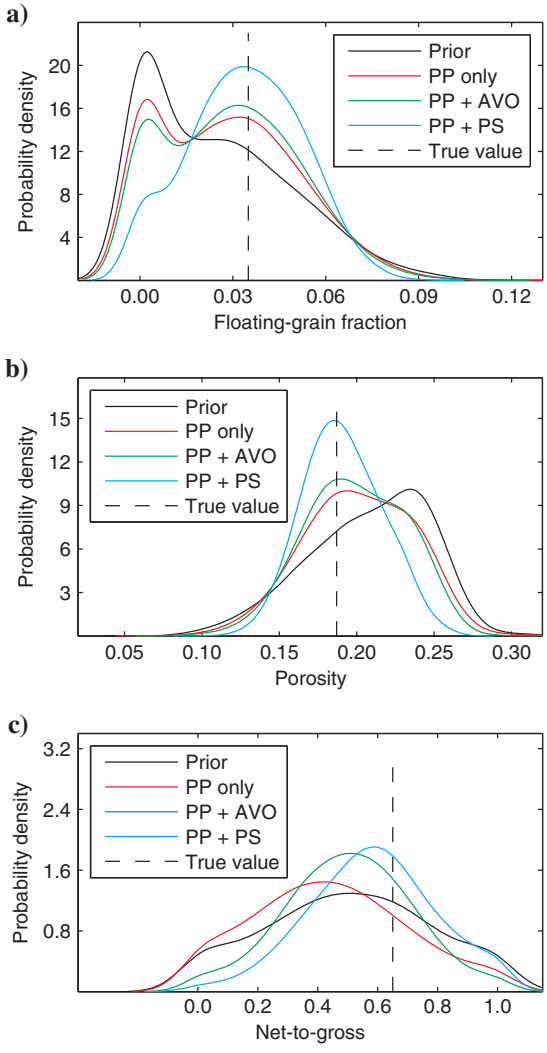

Figure 11. Posterior probability distributions of the (a) floating-grain fraction, (b) porosity, and (c) NG in the upper sand layer when the prior about NG is weak (i.e., $\mathrm{NG} \sim N(0.5, 0.3^2)$).

Downloaded 10/21/14 to 146.23.3.251. Redistribution subject to SEG license or copyright; see Terms of Use at http://library.seg.org/

gradient stacks or PS data leads to further reduction of the discrepancies, but adding the PS data gives the best results. For density, adding PS data does not lead to significant reduction in uncertainty. This is because, for the current case study, after conditioning to PP data, the uncertainty is already very small, leaving less room for further improvement.

Comparison of widths of uncertainty bounds

The MCMC-based methods also allow us to quantitatively compare the uncertainty associated with all the estimation. In this study, we calculate the widths of 95% predictive intervals. Similar to the comparison of the discrepancies, we normalize the results by those obtained from the prior PDFs.

Figure 14 shows the results for reservoir parameters and for effective parameters. For reservoir parameters (i.e., floating-grain fraction, porosity, and NG), the reduction of uncertainty is small and the maximum reduction is around 20%. The use of various combinations of seismic data does not seem to make a significant difference. For P-wave velocity and density, after conditioning to PP data, adding AVO gradient data or PS data does not lead further significant reduction. However, for S-wave velocity and layer thickness, adding PS data causes significantly more reduction in the uncertainty than adding AVO gradient data.

Comparison of predictive probabilities

In the previous subsections, we compare the discrepancies between the estimated and true value and the widths of uncertainty bounds, both of which just compare one aspect of posterior PDFs. A better evaluation is to compare the predictive probabilities of a small interval around the true value, which is given by

$$\text{prob}(\beta \in [(1-\varepsilon)\beta^{\text{true}}, (1+\varepsilon)\beta^{\text{true}}]|\text{data}), \qquad (29)$$

where β represents a variable under estimation. We set $\varepsilon = 2.5\%$ for effective density and 5% for other parameters because the posterior density has much smaller uncertainty compared with other effective

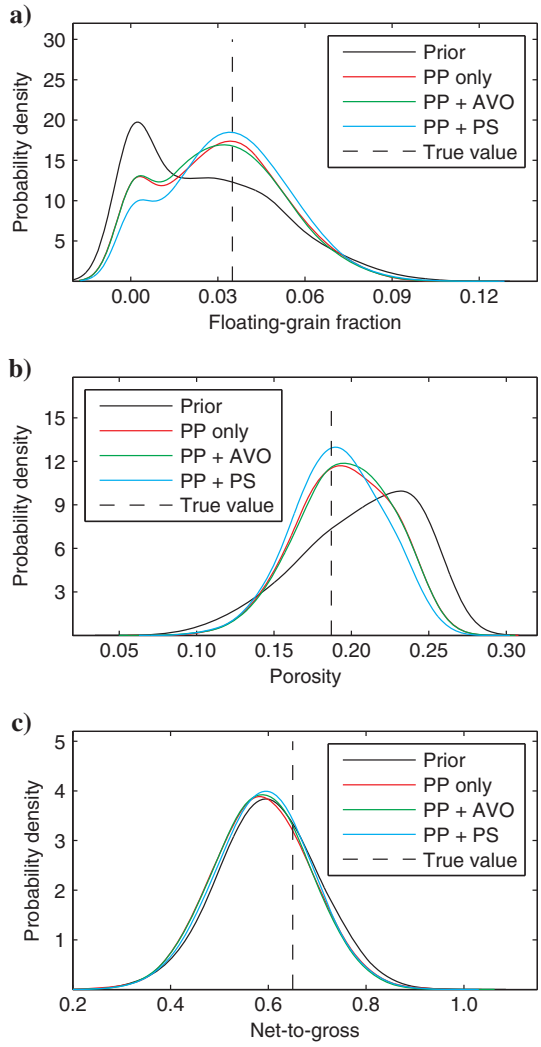

Figure 12. Posterior probability distributions of the (a) floating-grain fraction, (b) porosity, and (c) NG in the upper sand layer when the errors in the AVO gradient and PS data are doubled.

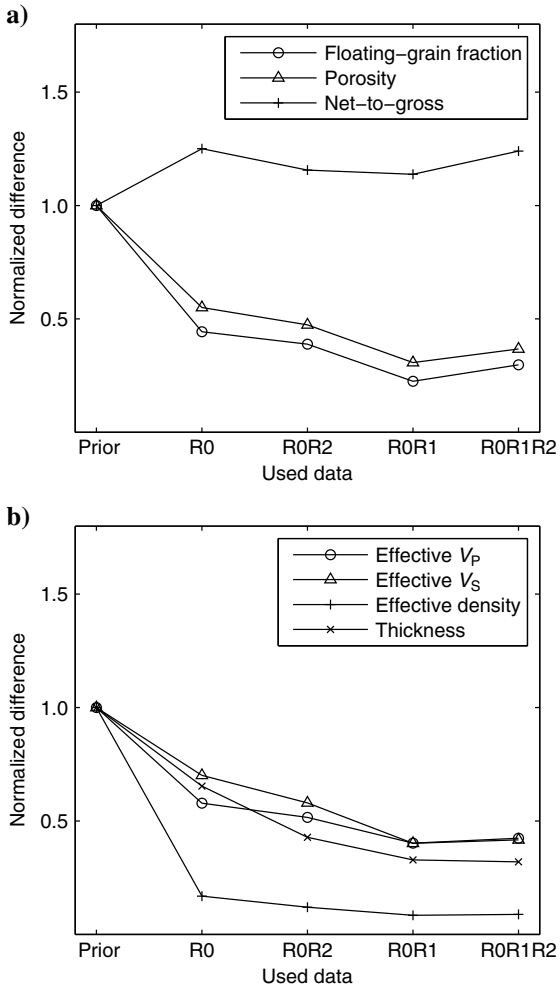

Figure 13. Comparison of differences between the true values and estimated medians for priors $X \sim N(0.0, 0.05^2)$, NG $\sim N(0.6, 0.1^2)$, and noise of 0.01 RFC for PP data and 0.02 RFC for others, in which R0 represents PP data only, R0R1 represents PP plus PS data, R0R2 represents PP plus AVO gradient data, and R0R1R2 represents all the data.

properties. A larger predictive probability means that the data provide stronger evidence to support the occurrence of the true values. Again, we normalize the probabilities by the prior predictive probability.

Figure 15a compares the predictive probability ratios of the floating-grain fraction, porosity, and NG. These results are more consistent than those shown in Figures 13a and 14a because the ratios of NG are very close to 1.0. This means that for the tight prior of NG (NG $\sim N(0.6, 0.1^2)$), the updating can be ignored. For the floating-grain fraction and porosity, the use of PP data significantly increases the predictive probabilities. Adding AVO gradient data does not cause significant improvement. However, adding PS data leads to significant improvement again. Figure 15b shows the comparison for effective P- and S-wave velocities, effective density, and layer thickness. Similarly, we found that adding PS data significantly improve the estimates of effective S-wave velocity and layer thickness compared with Figures 14b and 15b.

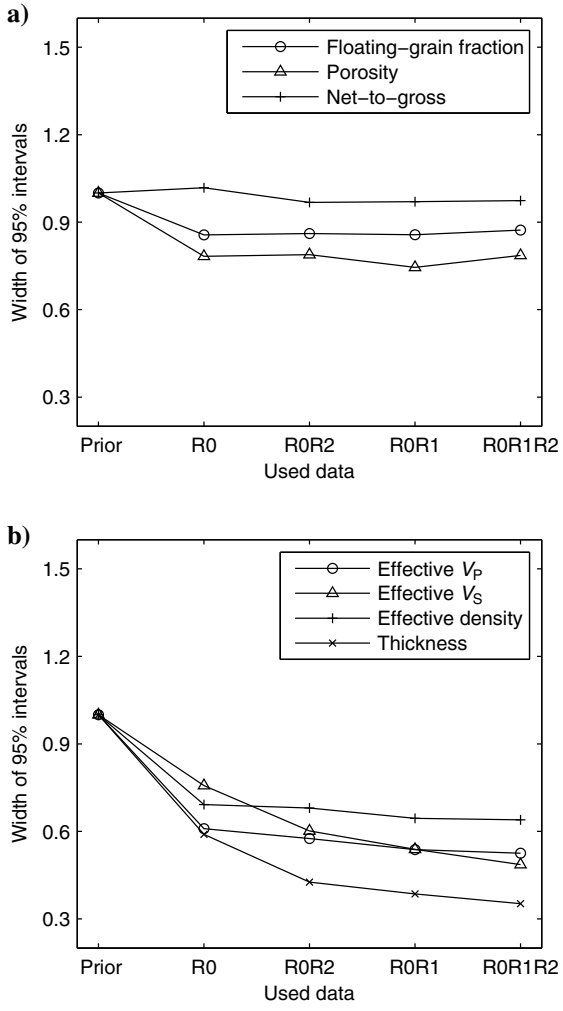

Figure 14. Comparison of half-widths of 95% predictive intervals for priors $X \sim N(0.0, 0.05^2)$, NG $\sim N(0.6, 0.1^2)$, and noise of 0.01 RFC for PP data and 0.02 RFC for others, in which R0 represents PP data only, R0R1 represents PP plus PS data, R0R2 represents PP plus AVO gradient data, and R0R1R2 represents all the data.

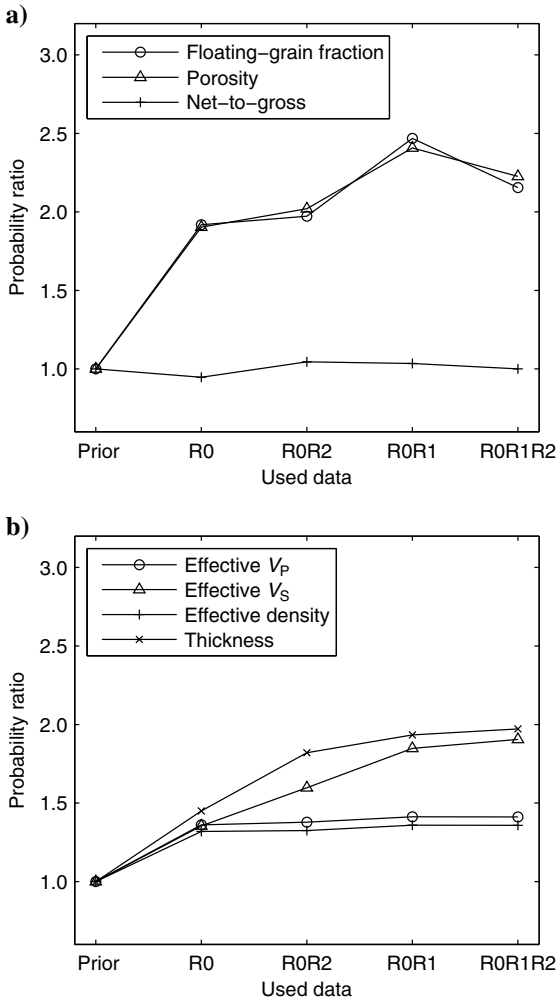

Figure 15. Comparison of predictive probability of the true values for priors $X \sim N(0.0, 0.05^2)$, NG $\sim N(0.6, 0.1^2)$, and noise of 0.01 RFC for PP data and 0.02 RFC for others, in which R0 represents PP data only, R0R1 represents PP plus PS data, R0R2 represents PP plus AVO gradient data, and R0R1R2 represents all the data.

CONCLUSIONS

We started from likelihood analysis of a simple two-layer model, with the first layer being shale and the second layer being sand, and we found that seismic PS data are significantly more informative than AVO gradient data, even with the high-order term included, for reservoir parameter estimation. Although this analysis is based on a floating-grain rock-physics model, it is straightforward to extend the method to other rock-physics models. We assume in this study that we have a suitable rock-physics model to link seismic attributes to reservoir parameters and that the seismic data are of reasonable quality. Without those assumptions, we may not be able to verify the benefits of using PS data.

We developed a hierarchical Bayesian model to combine PP and PS data for complicated situations (e.g., multiple layers, a large number of unknowns, etc.), motivated by the analytical results. We inverted PS data directly in the PS time domain unlike many previous methods, which first convert PS time to PP time and then

Downloaded 10/21/14 to 146.23.3.251. Redistribution subject to SEG license or copyright; see Terms of Use at http://library.seg.org/

Downloaded 10/21/14 to 146.23.3.251. Redistribution subject to SEG license or copyright; see Terms of Use at http://library.seg.org/

invert PS data in the PP time domain. The alignment of PP and PS time in our model is carried out by identifying one common reflection interface and using the PP and PS time to the common interface as references. This avoids many difficulties caused by the conversion of PS time to PP time, such as the distortion of wavelets, and the requirement of knowing internal P-wave to S-wave velocity ratios a priori.

We performed comparison studies based on a synthetic six-layer model to demonstrate the value of PS data for estimating reservoir parameters. PS data are very helpful for improving the estimates of porosity and the floating-grain fraction and for improving the estimates of effective S-wave velocity and layer-thickness under a range of priors and noise levels in seismic data. The NG is relatively less sensitive to PS data. Compared with the posterior results obtained from PP plus AVO gradient data, PP data are most informative for parameter estimation, then PS data, and finally AVO gradient data. This suggests that to improve the estimates of reservoir parameters, PS data are more valuable because PS data can provide complementary information to PP data and give similar but better information than AVO gradient data. Consequently, they have the potential of significantly improving parameter estimation results.

We claim that PS data are more informative than AVO gradient data for reservoir parameter estimation. To be precise, the PS data include some information from the matching between PP and PS time because we considered PS time registration as data in the model. The success of using PS data in the inversion depends on the existence of at least one reference PS time. In the cases in which we cannot find a good matching between PP and PS time, we may pick up multiple possible matching with uncertainty. Under these situations, the value of using PS data may be less apparent than what we have demonstrated in the six-layer models. In addition, because we used the convolution method for forward simulation of PP and PS responses, we need to have known PP and PS wavelets. This could be difficult in practice and thus limits the applicability of the current model.

ACKNOWLEDGMENTS

We thank Ion Geophysical for funding and for permission to publish this work. We thank J. Gunning from the Commonwealth Scientific and Industrial Research Organisation for providing help in understanding the Delivery codes and D. Sassen from Ion Geophysical for helping to answer some questions. We also thank S. Kaplan, H. H. Veire, M. Bosch, and one anonymous reviewer for their constructive comments.

APPENDIX A

DATA MATRICES FOR SYNTHETIC TWO-LAYER MODELS

For the case of using only PP data, we set $\mathbf{M}_d = (1, 0, 0)$. For the case of using PP and PS data, we set

$$\mathbf{M}_d = \begin{pmatrix} 1 & 0 & 0 \\ 0 & 1 & 0 \end{pmatrix}. \tag{A-1}$$

Similarly, for the case of using PP and AVO gradient traces, we set

$$\mathbf{M}_d = \begin{pmatrix} 1 & 0 & 0 \\ 0 & 0 & 1 \end{pmatrix}. \tag{A-2}$$

For the case of using all seismic data, we set

$$\mathbf{M}_d = \begin{pmatrix} 1 & 0 & 0 \\ 0 & 1 & 0 \\ 0 & 0 & 1 \end{pmatrix}. \tag{A-3}$$

APPENDIX B

DERIVATION OF MEAN VECTOR AND COVARIANCE MATRICES

In the current study, we assume that the reservoir parameters under estimation are the loading depth and floating-grain fraction. Let v_{pi}, v_{si}, ρ_i, z_i, and x_i be seismic P- and S-wave velocities, densities, loading depth, and floating-grain fraction at the ith layer, respectively. From the rock-physics model given in equations 1–5, we have

$$\begin{aligned}\mathbf{r}_i &= \begin{pmatrix} v_{\mathrm{pi}} \\ v_{\mathrm{si}} \\ \rho_i \end{pmatrix} = \begin{pmatrix} a_{\mathrm{vp}} \\ a_{\mathrm{vs}} + a_{\mathrm{vp}} b_{\mathrm{vs}} \\ a_\rho + a_{\mathrm{vp}} b_\rho \end{pmatrix} \\ &\quad + \begin{pmatrix} b_{\mathrm{vp}} & c_{\mathrm{vp}} \\ b_{\mathrm{vp}} b_{\mathrm{vs}} & c_{\mathrm{vp}} b_{\mathrm{vs}} \\ b_{\mathrm{vp}} b_\rho & c_{\mathrm{vp}} b_\rho + c_\rho \end{pmatrix} \begin{pmatrix} z_i \\ x_i \end{pmatrix} + \begin{pmatrix} \varepsilon_{\mathrm{vp}} \\ b_{\mathrm{vs}} \varepsilon_{\mathrm{vp}} + \varepsilon_{\mathrm{vs}} \\ b_\rho \varepsilon_{\mathrm{vp}} + \varepsilon_\rho \end{pmatrix} \\ &= \boldsymbol{\mu}_{\mathrm{ri}} + \mathbf{H}_i \boldsymbol{\alpha}_i + \boldsymbol{\varepsilon}_{\mathrm{ri}}. \end{aligned} \tag{B-1}$$

We can form vectors and matrices for all the layers by stacking those layer-based vectors and matrices; i.e., $\mathbf{r} = (\mathbf{r}_1^T, \mathbf{r}_2^T, \ldots, \mathbf{r}_n^T)^T$, $\boldsymbol{\mu}_r = (\boldsymbol{\mu}_1^T, \boldsymbol{\mu}_2^T, \ldots, \boldsymbol{\mu}_n^T)^T$, $\boldsymbol{\alpha} = (\boldsymbol{\alpha}_1^T, \boldsymbol{\alpha}_2^T, \ldots, \boldsymbol{\alpha}_n^T)^T$, $\boldsymbol{\varepsilon}_r = (\boldsymbol{\varepsilon}_1^T, \boldsymbol{\varepsilon}_2^T, \ldots, \boldsymbol{\varepsilon}_n^T)^T$, and $\mathbf{H} = (\mathbf{H}_1^T, \mathbf{H}_2^T, \ldots, \mathbf{H}_n^T)^T$.

It is straightforward to derive the covariance matrix from equation B-1 by assuming that residuals $\varepsilon_{\mathrm{vp}}$, $\varepsilon_{\mathrm{vs}}$, and ε_ρ in equations 1–3 have Gaussian distributions with zero mean and variances of σ_{vp}^2, σ_{vs}^2, and σ_ρ^2, respectively. Specifically, the matrix is

$$\boldsymbol{\Sigma}_{\mathrm{ri}} = \sigma_{\mathrm{vp}}^2 \begin{pmatrix} 1 & b_{\mathrm{vs}} & b_\rho \\ b_{\mathrm{vs}} & b_{\mathrm{vs}}^2 + \sigma_{\mathrm{vs}}^2/\sigma_{\mathrm{vp}}^2 & b_{\mathrm{vs}} b_\rho \\ b_\rho & b_{\mathrm{vs}} b_\rho & b_\rho^2 + \sigma_\rho^2/\sigma_{\mathrm{vp}}^2 \end{pmatrix}. \tag{B-2}$$

The covariance matrix $\boldsymbol{\Sigma}_r = \mathrm{diag}\,(\boldsymbol{\Sigma}_{\mathrm{r1}}, \boldsymbol{\Sigma}_{\mathrm{r2}}, \ldots, \boldsymbol{\Sigma}_{\mathrm{rn}})$.

REFERENCES

Aki, K., and P. G. Richards, 1980, Quantitative seismology: Theory and methods: W. H. Freeman and Co.

Bale, R., T. Marchand, K. Wilkinson, K. Wikel, and R. Kendall, 2013, The signature of shear-wave splitting: Theory and observations on heavy oil data: The Leading Edge, **32**, 14–24, doi: 10.1190/tle32010014.1.

Bansal, R., and M. Matheney, 2010, Wavelet distortion correction due to domain conversion: Geophysics, **75**, no. 6, V77–V87, doi: 10.1190/1.3494081.

Bernardo, J. M., and F. M. Smith, 2000, Bayesian theory: John Wiley & Sons.

Brettwood, P., J. P. Leveille, and S. Singleton, 2013, C-wave data improve seismic imaging: The American Oil & Gas Reporter, **1**, 1–5.
Castagna, J. P., H. W. Swan, and D. J. Foster, 1998, Framework for AVO gradient and intercept interpretation: Geophysics, **63**, 948–956, doi: 10.1190/1.1444406.
Chen, J., A. Kemna, and S. Hubbard, 2008, A comparison between Gauss-Newton and Markov chain Monte Carlo based methods for inverting spectral induced polarization data for Cole-Cole parameters: Geophysics, **73**, no. 6, F247–F259, doi: 10.1190/1.2976115.
Davis, T. L., A. Bibolova, S. O'Brien, D. Klepacki, and H. Robinson, 2013, Prediction of residual oil saturation and cap-rock integrity from time-lapse, multicomponent seismic data, Delhi field, Louisiana: The Leading Edge, **32**, 26–31, doi: 10.1190/tle32010026.1.
DeMartini, D. C., and M. E. Glinsky, 2006, A model for variation of velocity versus density trends in porous sedimentary rocks: Journal of Applied Physics, **100**, 014910, doi: 10.1063/1.2210171.
Gardner, G. H. F., L. W. Gardner, and A. R. Gregory, 1974, Formation velocity and density — The diagnostic basics for stratigraphic traps: Geophysics, **39**, 770–780, doi: 10.1190/1.1440465.
Glinsky, M. E., A. Cortis, D. Sassen, H. Rael, and J. Chen, 2013, Rock physics and geophysics for unconventional resources, multicomponent seismic, quantitative interpretation: Presented at 2nd International Workshop on Rock Physics, http://arxiv.org/abs/1304.6048, accessed 4–9 August 2013.
Gunning, J., and M. E. Glinsky, 2004, Delivery: An open-source model-based Bayesian seismic inversion program: Computers and Geosciences, **30**, 619–636, doi: 10.1016/j.cageo.2003.10.013.
Gunning, J., and M. E. Glinsky, 2007, Detection of reservoir quality using Bayesian seismic inversion: Geophysics, **72**, no. 3, R37–R49, doi: 10.1190/1.2713043.
Hardage, B. A., M. V. DeAngelo, P. E. Murray, and D. Sava, 2011, Multicomponent seismic technology: SEG, Geophysical References Series.
Mahmoudian, F., and G. F. Margrave, 2004, Three-parameter AVO inversion with PP and PS data using offset-binning: CREWES Report, vol. 16.
Pacal, E. E., 2012, Seismic imaging with ocean-bottom nodes (OBNs): New acquisition designs and the Atlantis 4C OBN: M.S. thesis, University of Houston.
Rodriguez-Saurez, C., 2000, Advanced marine methods: Ocean-bottom and vertical cable analyses: Ph.D. thesis, University of Calgary.
Stewart, R. R., J. E. Gaiser, R. J. Brown, and D. C. Lawton, 2002, Tutorial — Converted-wave seismic exploration: Methods: Geophysics, **67**, 1348–1363.
Stone, C. J., 1995, A course in probability and statistics: Duxbury Press.
Veire, H. H., and M. Landrø, 2006, Simultaneous inversion of PP and PS seismic data: Geophysics, **71**, no. 3, R1–R10, doi: 10.1190/1.2194533.
Venables, W. N., and B. D. Ripley, 1999, Modern applied statistics with S-Plus 3rd ed.: Springer.

Downloaded 10/21/14 to 146.23.3.251. Redistribution subject to SEG license or copyright; see Terms of Use at http://library.seg.org/